Electronic Supplementary Material (ESI) for Environmental Science: Nano.

Supporting Information for

Discovery and potential ramifications of reduced iron-bearing nanomaterials—magnetite, wüstite, and zero valent iron—in wildland-urban interface fire ashes

Mohammed Baalousha[1*], Morgane Desmau[2], Sheryl A. Singerling[3], Jackson P. Webster[4], Sandrine J. Matiasek[5], Michelle A. Stern[6], and Charles N. Alpers[6]

[1] Center for Environmental Nanoscience and Risk, Department of Environmental Health Sciences, Arnold School of Public Health, University of South Carolina, Columbia, South Carolina, United States

[2] Deutsches Elektronen-Synchrotron DESY, Notkestr. 85, 22607 Hamburg, Germany

[3]NanoEarth, Institute for Critical Technology and Applied Science, Virginia Polytechnic Institute and State University, Blacksburg, Virginia, United States

[4] Department of Civil Engineering, California State University Chico, 400 W 1st St, Chico, CA 95929, United States

[5] Department of Earth and Environmental Sciences, California State University Chico, 400 W 1st St, Chico, CA 95929, United States

[6] U.S. Geological Survey, California Water Science Center, 6000 J Street, Sacramento, CA 95819, United States

* Corresponding author: mbaalous@mailbox.sc.edu

Table S1. Description of ashes collected following the 2020 fire season. Samples analyzed by TEM are highlighted in gray.

Sample number	Sampling date	Ash Source	Sample description
Lightning Complex Fire			
A11	10/7/2020	Structure/Residential	Burned shed
A12	10/7/2020	Structure/Residential	Burned shed - replicate
A13	10/7/2020	Vehicle	Burned trailer - south end
A14	10/7/2020	Vehicle	Burned trailer - north end
A21	10/7/2020	Structure/Residential	Back room
A22	10/7/2020	Structure/Residential	Front room
A23	10/7/2020	Structure/Residential/kitchen	Kitchen area
A24	10/7/2020	Structure/Foundation	Dark green material on foundation (Cu arsenate?)
A25	10/7/2020	Structure/Residential	Tool shed - separated from house
A91	10/15/2020	Structure/Residential	Hot tub / spa
A92	10/15/2020	Structure/Residential	Red soil - artificial wood from deck
A93	10/15/2020	Structure/Residential/kitchen	Kitchen area, copper wires
A94	10/15/2020	Structure/Garage	Garage-1, electronics, copper wires, other blue material, misc. ash
A95	10/15/2020	Structure/Garage	Garage-2, metal wires, misch ash
A96	10/15/2020	Structure/Residential	Other parts of house, some electronics (Cu), some CCA treated wood.
A121	10/15/2020	Structure/Residential	Burned residence - some copper wire, mostly white ash (wallboard)
A122	10/15/2020	Structure/Residential/paint	Studio - some burned paint (acrylic and watercolor) blues, yellow, red
A123	10/15/2020	Structure/Residential	Studio - misc. ash, some wires
A124	10/15/2020	Structure/Residential/paint	Shed - house paint, some wires
A125	10/15/2020	Structure/Foundation	Olive green ash from foundation, some yellow crystals replacing wallboard
A131	10/16/2020	Structure/vehicle	Burned barn - redwood, galvanized steel, tires, Cu wire
A132	10/16/2020	Structure/vehicle	Burned tool storage shed - tires, white & black ash, misc. bags & containers
A133	10/16/2020	Structure/Residential	Burned farm worker residence - white & black ash; mattress, sink, refrigerator
A134	10/16/2020	Vehicle	Burned boat & trailer - fiberglass, aluminum, tires
A135	10/16/2020	Structure/vehicle	Burned farm workshop - tools, Cu wire, tractor, tires; some blue pigments 2 shades), black, white, red & brown ash; white powder
A136	10/16/2020	Vehicle	Burned trailer (for 2 horses?) - tires, Cu wire, aluminum, book (manual?)
A137	10/16/2020	Structure/Residential	Burned farmworker residence - black, white & brown ash
A138	10/16/2020	Structure/Residential	Burned 1-story residence (occupied) -- white, gray & red ash; burned guns
A139	10/16/2020	Structure/Residential	Burned 2-story residence (unoccupied) -- white, brown & red ash (kitchen)
A141	10/16/2020	Structure/Commercial	North end of store - gray & white ash, fiberglass, dry wall, beverage containers
A142	10/16/2020	Structure/Commercial/Electronics	South end of store - Electronics (PC and calculator?), Cu wires, white & gray ash
A143	10/16/2020	Structure/Commercial	Storage building - Gray & white ash, Cu wiring (2 shades of green)
A31	10/8/2020	Vegetation	Burned chaparral (charred manzanita and some pine) site on gentle slopes; serpentinite unit
A51	10/8/2020	Vegetation	Burned chapparal (manzanita), white ash with some black ash; sandstone unit
A81	10/8/2020	Vegetation	Burned oak, white ash with some black ash; bedrock undetermined

North Complex Fire			
AD		Atmospheric deposition	Ash deposited on a car windshield
NC-01	10/7/2020	Vegetation	White ash from edge of Lake Madrone (west shore)
NC01-A	10/7/2020	Vegetation	White ash appears to be remnants of dead tree. Very light and fluffy.
NC01-B	10/7/2020	Vegetation	Black ash from surface of soil. Appears to be duff layer
NC01-C	10/7/2020	Soil	Scraped ash away from surface soil and collected 0-2 cm. Soil was a clay rich, red-orange color, very dense. We could not dig down with the plastic scoop (dry clay)
NCWZ-02	10/7/2020	Structure/Residential	House "ash" collected from bedroom or living room area. Removed large tile material and collected from below large pieces
NC04-A	10/7/2020	Structure/Garage	White ash from auto garage containing many tools. Collected from a large pile of sifted ash in center of garage
NC04-B	10/7/2020	Vehicle	Composite car ash
NC04-C	10/7/2020	Vehicle	Tire material (collected in glass for organic analysis)
NC06-A	10/7/2020	Soil	Soil 0-2 cm
NC06-B	10/7/2020	Soil	Soil 10-15 cm
NC06-C	10/7/2020	Vegetation	Ash from soil surface
NC-08	10/7/2020	Structure/Residential	Composite sample of cabin built in 1930's era
NC-09	10/7/2020	Vehicle	Golf cart ash composite
NC10-A	10/7/2020	Structure/Residential	Cabin. Composite sample collected from inside foundation.
NC10-B	10/7/2020	Soil	Surface soil/ash collected 5 ft outside of foundation, adjacent to building
NC11-A	10/7/2020	Vehicle	Car ash, composite from ground, early 2000's Ford Mustang
NC11-B	10/7/2020	Vehicle	Car ash, interior
NC12-A	10/7/2020	Vegetation	Ash from pine forest. High severity. Above reservoir.
NC12-B	10/7/2020	Soil	Soil 0-2 cm
NC12-C	10/7/2020	Soil	Soil 10-15cm

Soil description

Soils in the North Complex Fire area

Most soils around Madrone Lake are in the Islandbar series (primarily decomposed granite)

94

NCWZ 12: Soil classification 209 – ISLANDBAR SERIES

The Islandbar series consists of very deep, somewhat excessively drained soils that formed in residuum and colluvium from coarse grained intrusive igneous rocks, mainly trondhjemite or quartz diorite. Islandbar soils are on ridge tops and side slopes on granitic Sierra Nevada. Slopes range from 2 to 70%. The mean annual precipitation is about 1473 mm and the mean annual temperature is about 13 ºC.

TAXONOMIC CLASS: Coarse-loamy, mixed, active, mesic Typic Dystroxerepts

TYPICAL PEDON: Islandbar sandy loam, on a northwest facing 5 percent slope under a cover of conifers, hardwoods, and shrubs at an elevation of 677 m. When described on 7/22/1998, the soil was dry to a depth of 91 cm and was slightly moist from 91 to 183 cm. (Colors are for dry soil unless otherwise noted).

Oi--0 to 5 cm; slightly decomposed plant material; abrupt smooth boundary.

A1--5 to 13 cm; light brownish gray (10YR 6/2) sandy loam, dark grayish brown (10YR 4/2) moist; 12% clay; weak fine subangular blocky parting to weak fine granular structure; slightly hard, very friable, nonsticky, nonplastic; many very fine and fine roots; many very fine and fine irregular pores; 5 percent mica flakes; 5 percent rounded gravel; moderately acid, pH 6.0 by Hellige-Truog; abrupt smooth boundary.

NCWZ 1, NCWZ 6, and NCWZ 10B: Soil classification 202 – Holland Series

The Holland series consists of very deep, well drained soils that formed in material weathered from granitic rock. Holland soils are on foothills and low mountains and have slopes of 2 to 75%. The mean annual precipitation is about 940 mm and the mean annual air temperature is about 13 ºC.

TAXONOMIC CLASS: Fine-loamy, mixed, active, mesic Ultic Haploxeralfs

TYPICAL PEDON: Holland sandy loam - on an east facing, linear, slope of 25% under ponderosa pine, incense cedar, and mountain misery at an elevation of 1145 m. (Colors are for dry soil unless otherwise noted. When described August 24, 1977, the soil was slightly moist throughout).

Oi--0 to 5 cm; fresh and decomposing pine needle and leaf litter.

A1--5 to 13 cm; brown (10YR 5/3) sandy loam, very dark grayish brown (10YR 3/2) moist; 17% clay; strong fine granular structure; soft, very friable, slightly sticky and slightly plastic; many very fine and fine roots; many very fine interstitial, common fine tubular pores; moderately acid (pH 5.7); abrupt wavy boundary. (5 to 15 cm thick)

NCWZ 13: Soil classification – Hartsmill Series

The Hartsmill series consists of very deep, well drained soils that formed in colluvium and residuum from metavolcanic rocks, mainly greenschist. Hartsmill soils are on ridge tops and side slopes on metamorphic Sierra Nevada foothills. Slopes range from 2 to 90%. The mean annual precipitation is about 43 inches, (109 cm) and the mean annual temperature is about 14 ºC.

TAXONOMIC CLASS: Loamy-skeletal, mixed, superactive, thermic Ultic Palexeralfs

TYPICAL PEDON: Hartsmill gravelly loam, on a southwest facing 46 percent slope under a cover of whiteleaf manzanita (*Arctostaphylos manzanita*), toyon (*Heteromeles arbutifolia*), interior live oak (*Quercus wislizeni*), California black oak (*Quercus kelloggii*), Pacific poison oak (*Toxicodendron diversilobum*) and very scattered ponderosa pine (*Pinus ponderosa*) at an

elevation of 1,840 feet, (561 m). When described on 7/27/1999, the soil was dry throughout. (Colors are for dry soil unless otherwise noted).

Oi--0 to 3 cm; slightly decomposed plant material; abrupt smooth boundary.

A--3 to 8 cm; reddish brown (5YR 4/4) gravelly loam, dark reddish brown (5YR 3/3), moist; 14% clay; strong fine granular structure; soft, very friable, nonsticky, slightly plastic; common very fine roots; many very fine irregular pores; 30 percent angular gravel; slightly acid, pH 6.5 by Hellige-Truog; abrupt smooth boundary. 5 to 8 cm thick).

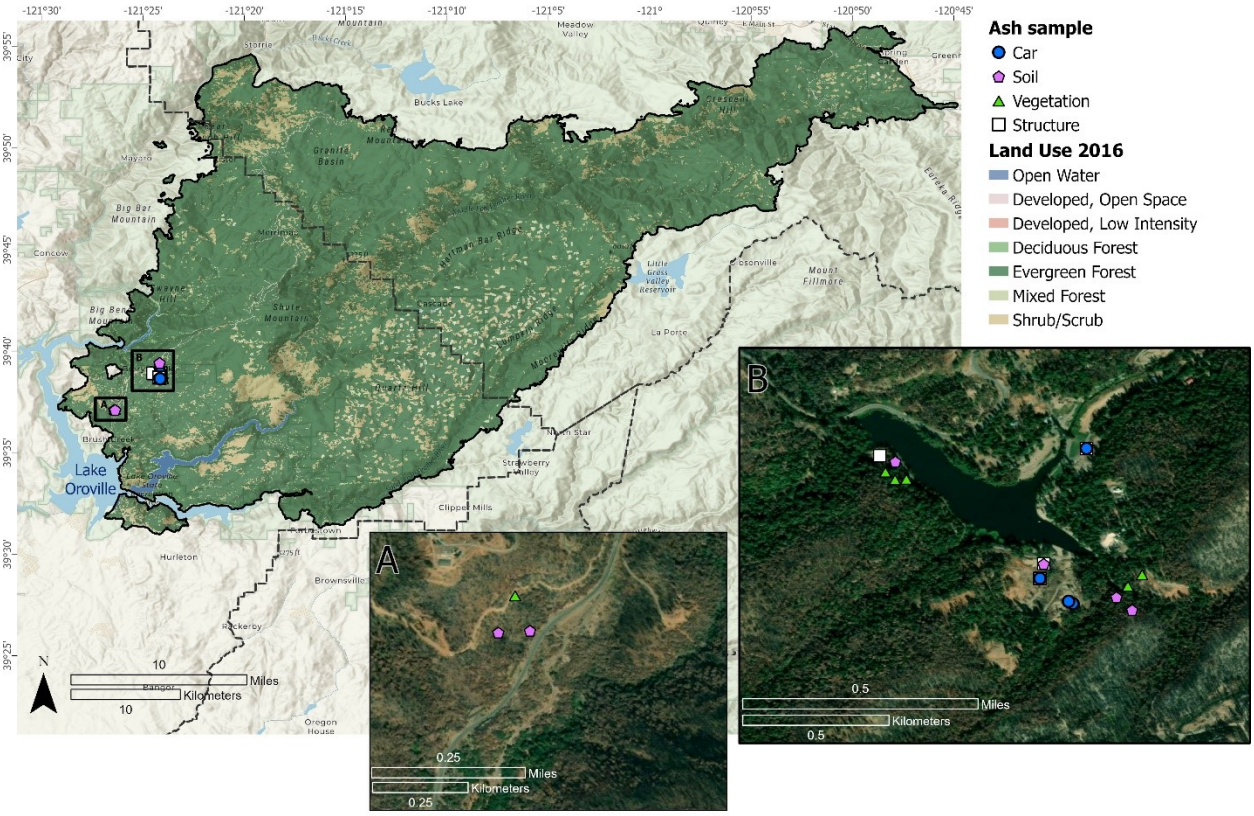

Figure S1. Land use classification for the North Complex fire and approximate locations of ash samples.

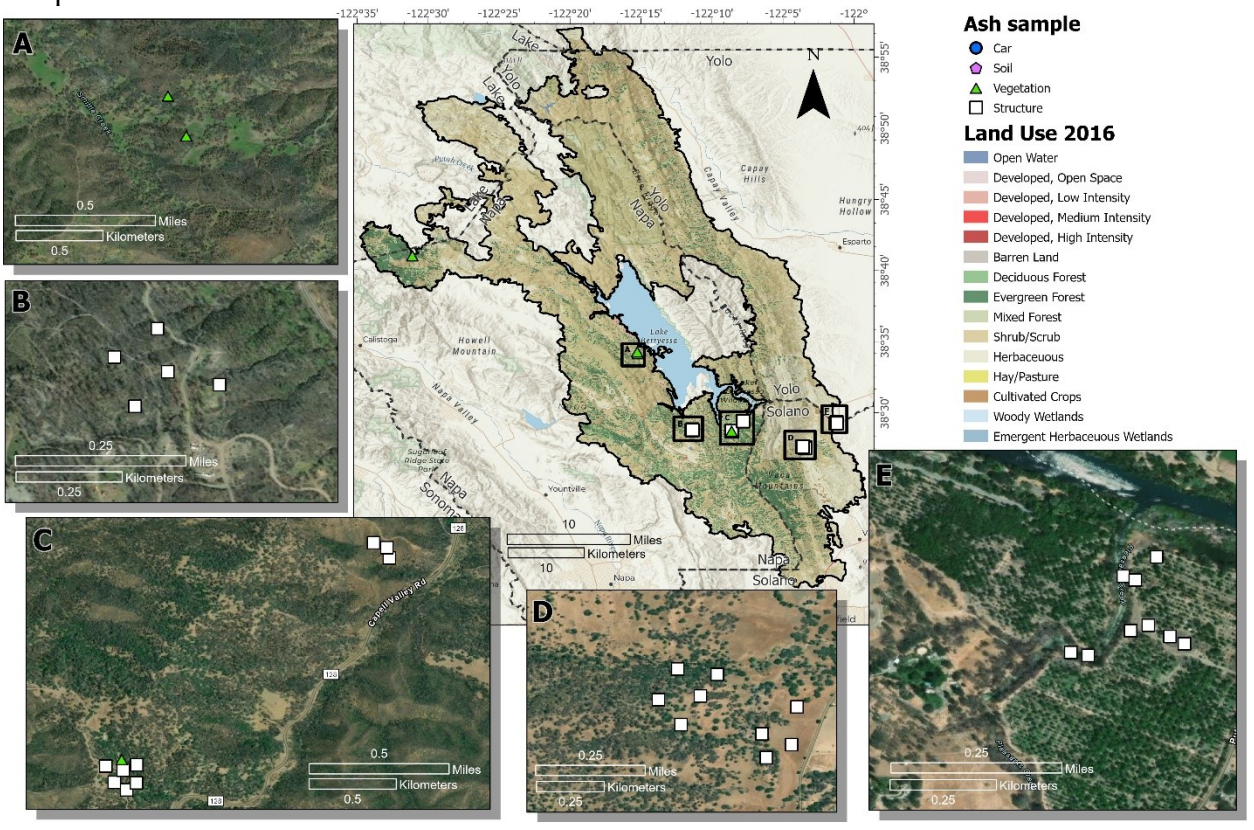

Figure S2. Land use classification for the LNU Lightning Complex fire and approximate locations of ash samples.

Figure S3. Collection of residential structure ash and soil samples

Synthesis of Goethite

Goethite was synthesized using an aqueous aging of ferrihydrite modified method after Schwertmann et al. (1985) [51]. Sodium hydroxide solution (5 M, 120 ml) was added dropwise to an iron (III) nitrate solution (1 M, 200 ml). The resulting ferrihydrite suspension was basified by dropwise addition of sodium hydroxide (5 M) until pH 12 was achieved. The bottle was then closed and heated in a furnace for 3 days. The initial temperature was 50 °C, however, this was increased to 60 °C after the first day of the reaction. The product was recovered by centrifugation. The product was then washed four times and let to dry.

Synthesis magnetite and maghemite

Magnetite nanoparticles were synthetized by aqueous coprecipitation of ferric and ferrous iron in an anaerobic chamber in strict anaerobic conditions in pH 12 deionized water. Magnetite nanoparticles were then vacuum-dried on 0.2 μm cellulose filter and washed with O_2-free deionized water. Average diameter is 10.0 ± 1.4 nm, determined by High Resolution Transmission Electron Microscopy (HR-TEM). X-ray diffraction (XRD) was used to check the purity of the phase, it indicated a pure magnetite phase with a mean coherent domain size of 12.7 nm.

Maghemite nanoparticles were obtained by heating the previously described nanoparticles at 200°C during one night in strict anaerobic conditions. XRD indicated a pure maghemite phase with a 11.4 nm mean coherent domain size and an average diameter size of 10.3 ± 2.7 nm (HR-TEM).

Synthesis of Hematite

Hematite was synthesized by aqueous precipitation of ferric iron. Sodium hydroxide solution (5 M) was added dropwise to an iron (III) nitrate solution (1 M) until pH 7 was achieved. The resulting hematite solution was washed with Milli-Q water several times. The pH is then

adjusted again to 7 using NaOH (1M). The bottle was then closed and heated in a furnace at 80 °C. The product was recovered by centrifugation. The product was then washed four times and let to dry.

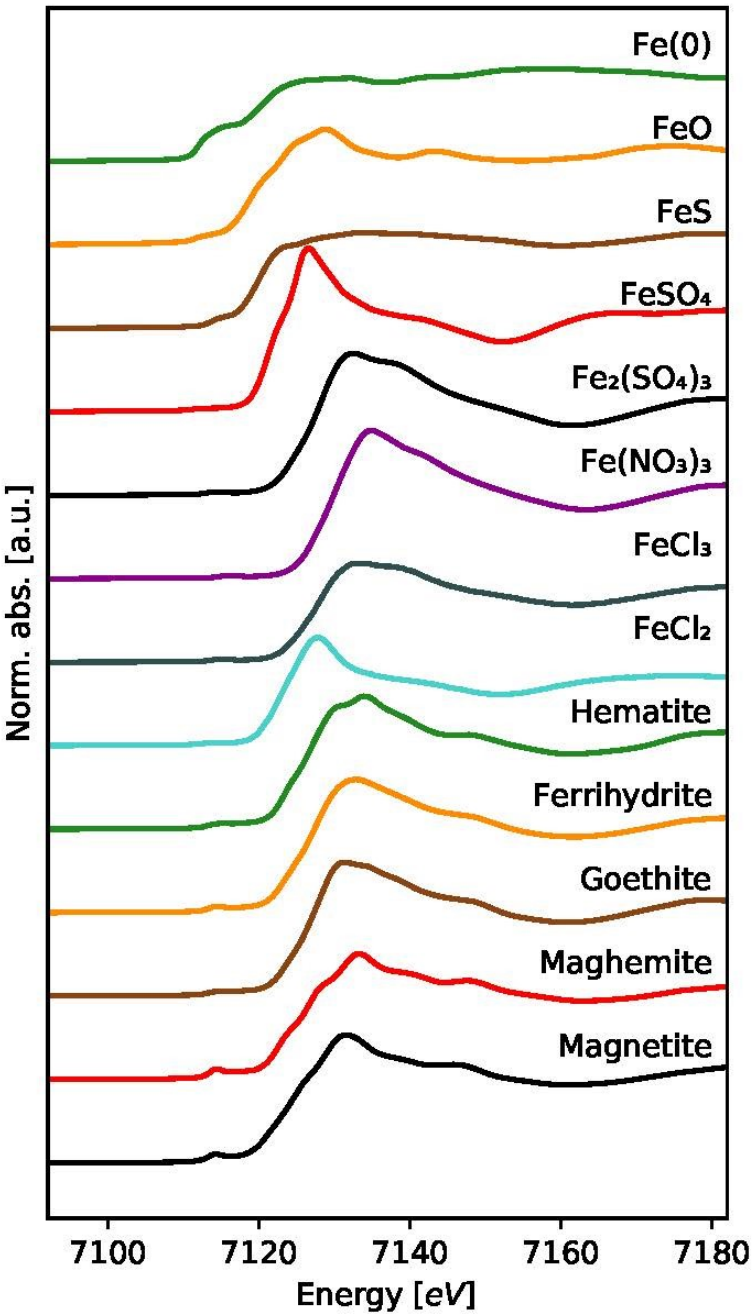

Figure S4. Iron K-edge XANES spectra of the model compound used to fit the iron K-edge XANES spectra of the fire ashes.

Table S2. Spectral weight of the different iron oxide phases and oxidation states together with the best fit error

Iron oxidation state	Fe(III)							Fe(III)/Fe(II)	Fe(II)				Fe(0)	χ_2
Iron species	Ferrihydrite	Maghemite	Goethite	Hematite	Fe(III)chlorite	Fe(III)nitrate	Fe(III)sulfate	Magnetite	FeS	Fe(II)chlorite	FeO	Fe(II)sulfate	Elemental Fe	
A11	25 ± 3	75 ± 3	0	0	0	0	0	0	0	0	0	0	0	0.021
A12	0	84 ± 2	0	0	0	0	16 ± 2	0	0	0	0	0	0	0.053
A13	65 ± 7	0	0	0	0	0	0	35 ± 6	0	0	0	0	0	0.039
A14	21 ± 4	26 ± 2	0	0	16 ± 1	0	0	37 ± 4	0	0	0	0	0	0.015
A21	51 ± 2	35 ± 2	0	0	0	0	0	0	0	0	0	0	14 ± 1	0.030
A22	0	53 ± 2	23 ± 2	0	0	0	0	0	14 ± 1	10 ± 1	0	0	0	0.018
A23	63 ± 4	14 ± 4	0	0	0	0	0	0	13 ± 1	0	0	0	10 ± 1	0.028
A24	0	78 ± 1	0	0	22 ± 1	0	0	0	0	0	0	0	0	0.034
A25	0	69 ± 3	0	0	165 ± 1	0	0	15 ± 2	0	0	0	0	0	0.022
A91	0	0	19 ± 2	0	0	0	0	81 ± 2	0	0	0	0	0	0.041
A92	0	90 ± 1	0	0	0	0	0	0	0	10 ± 1	0	0	0	0.049
A93	0	15 ± 2	0	0	0	0	0	46 ± 2	15 ± 1	23 ± 1	0	0	0	0.011
A94	0	47 ± 2	0	0	0	0	0	53 ± 2	0	0	0	0	0	0.029
A95	13 ± 3	38 ± 3	0	0	0	0	0	50 ± 2	0	0	0	0	0	0.027
A96	0	35 ± 3	0	0	0	0	0	24 ± 4	0	0	15 ± 1	26 ± 1	0	0.040
A121	0	35 ± 3	0	0	0	0	0	48 ± 3	0	17 ± 1	0	0	0	0.029
A122	0	40 ± 2	0	0	0	0	0	44 ± 3	0	0	0	16 ± 1	0	0.015
A123	49 ± 3	30 ± 3	0	0	0	0	0	0	0	10 ± 1	0	0	10 ± 1	0.020
A124	0	50 ± 1	0	50 ± 1	0	0	0	0	0	0	0	0	0	0.006
A125	0	51 ± 2	0	0	0	0	0	31 ± 2	18 ± 1	0	0	0	0	0.019
A131	21 ± 2	50 ± 2	0	0	0	0	0	29 ± 1	0	0	0	0	0	0.010
A132	0	38 ± 4	0	0	10 ± 1	0	0	52 ± 3	0	0	0	0	0	0.041
A133	0	45 ± 2	0	0	10 ± 1	0	0	32 ± 3	0	0	0	13 ± 1	0	0.015
A134	0	53 ± 2	26 ± 2	0	0	0	0	0	21 ± 1	0	0	0	0	0.024
A135	0	46 ± 2	36 ± 2	0	0	0	0	0	19 ± 1	0	0	0	0	0.027
A136	0	21 ± 2	44 ± 1	0	0	0	0	35 ± 2	0	0	0	0	0	0.017
A137	0	57 ± 3	0	0	0	0	0	32 ± 3	0	11 ± 1	0	0	0	0.014
A138	0	34 ± 2	20 ± 2	0	0	0	0	46 ± 2	0	0	0	0	0	0.029
A139	0	44 ± 2	0	0	0	0	0	45 ± 3	0	0	0	12 ± 1	0	0.018
A141	0	0	0	0	0	0	0	65 ± 1	22 ± 1	23 ± 1	0	0	0	0.011
A142	25 ± 3	26 ± 3	0	0	0	0	0	27 ± 3	13 ± 1	0	0	10 ± 1	0	0.013
A143	42 ± 2	14 ± 2	0	0	0	0	0	35 ± 2	10 ± 1	0	0	0	0	0.011
A031	17 ± 3	33 ± 4	0	0	0	0	0	33 ± 4	0	17 ± 2	0	0	0	0.040
A051	0	44 ± 2	0	0	13 ± 1	0	0	28 ± 2	0	15 ± 1	0	0	0	0.013
A081	0	43 ± 2	0	0	10 ± 1	0	0	47 ± 1	0	0	0	0	0	0.012
AD	0	33 ± 3	0	0	0	0	0	57 ± 3	0	0	0	10 ± 1	0	0.025
NC-1	0	32 ± 3	0	18 ± 2	0	0	0	50 ± 2	0	0	0	0	0	0.029
NC-1A	0	50 ± 2	33 ± 1	0	0	0	0	17 ± 2	0	0	0	0	0	0.022
NC-1B	24 ± 5	20 ± 4	0	31 ± 4	0	0	0	25 ± 5	0	0	0	0	0	0.038
NC-1C	16 ± 7	43 ± 3	0	25 ± 4	15 ± 2	0	0	0	0	0	0	0	0	0.033
NC-2	33 ± 3	0	0	0	0	0	0	31 ± 4	0	0	21 ± 1	15 ± 1	0	0.020
NC-4B	20 ± 2	0	0	0	0	0	0	63 ± 2	17 ± 1	0	0	0	0	0.018
NC-4C	0	34 ± 2	0	31 ± 3	35 ± 1	0	0	0	0	0	0	0	0	0.028
NC-6A	0	34 ± 2	0	31 ± 3	35 ± 1	0	0	0	0	0	0	0	0	0.028
NC-6B	0	26 ± 2	0	48 ± 3	25 ± 1	0	0	0	0	0	0	0	0	0.015
NC-6C	0	29 ± 3	16 ± 5	35 ± 6	0	0	0	21 ± 2	0	0	0	0	0	0.037
NC-8	0	60 ± 3	0	0	0	0	0	29 ± 4	0	0	0	11 ± 1	0	0.038
NC-9	0	36 ± 3	0	0	0	0	0	54 ± 4	0	10 ± 2	0	0	0	0.044
NC-10A	15 ± 3	39 ± 4	0	0	0	0	0	33 ± 4	0	0	0	13 ± 1	0	0.034
NC-10B	0	25 ± 3	0	0	0	0	0	58 ± 4	0	0	0	18 ± 1	0	0.042
NC-11A	0	0	0	0	0	0	0	48 ± 1	17 ± 2	0	20 ± 3	16 ± 2	0	0.045
NC-11B	0	0	0	0	0	0	0	26 ± 1	21 ± 1	0	53 ± 1	0	0	0.016
NC-12A	0	0	0	0	0	11 ± 1	0	58 ± 2	0	30 ± 1	0	0	0	0.018
NC-12B	19 ± 6	16 ± 2	42 ± 4	0	0	0	0	0	0	23 ± 1	0	0	0	0.008
NC-12C	0	25 ± 1	54 ± 1	0	0	0	0	0	0	21 ± 1	0	0	0	0.009

6.

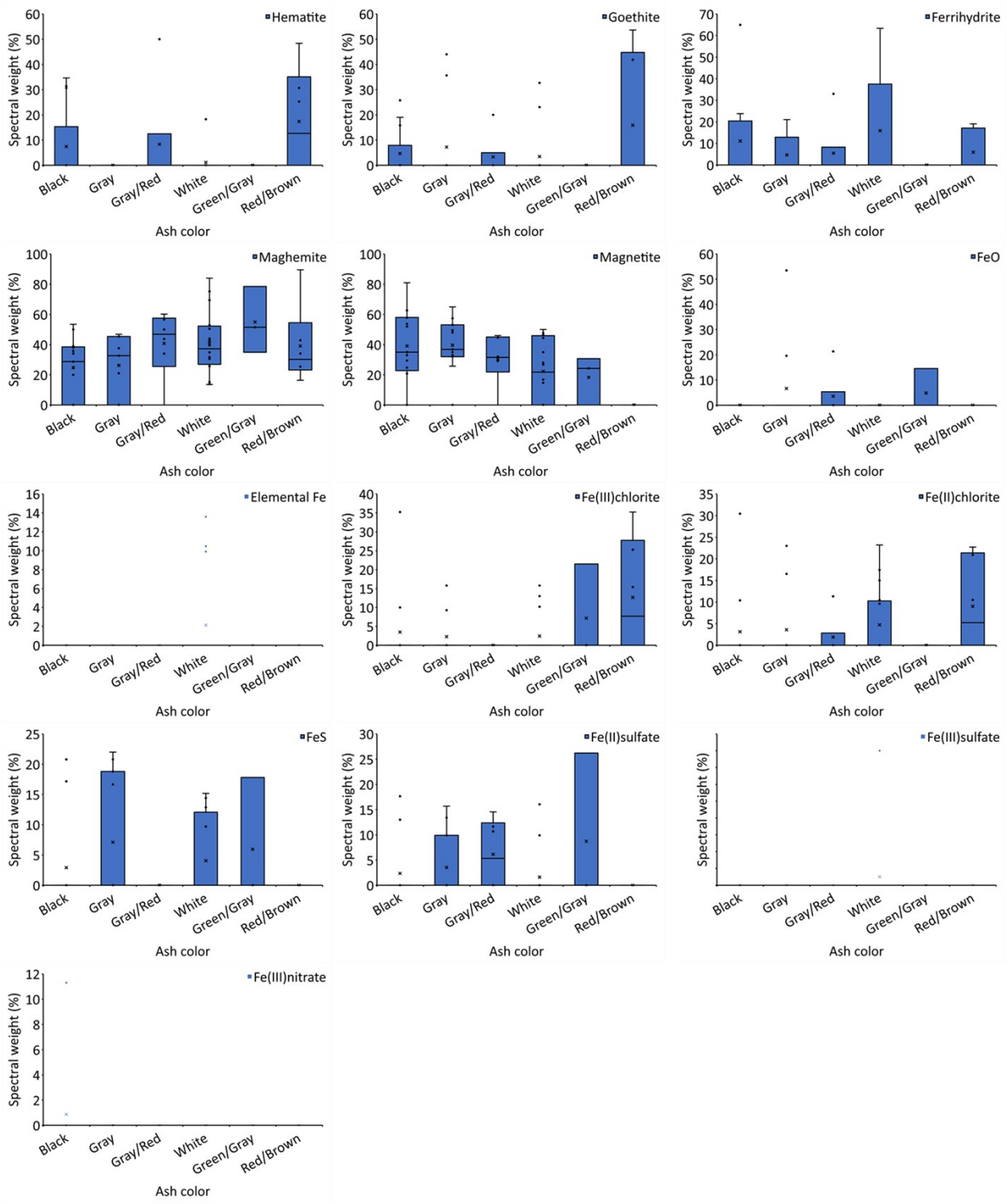

Figure S5. Iron phases as a function of ash color

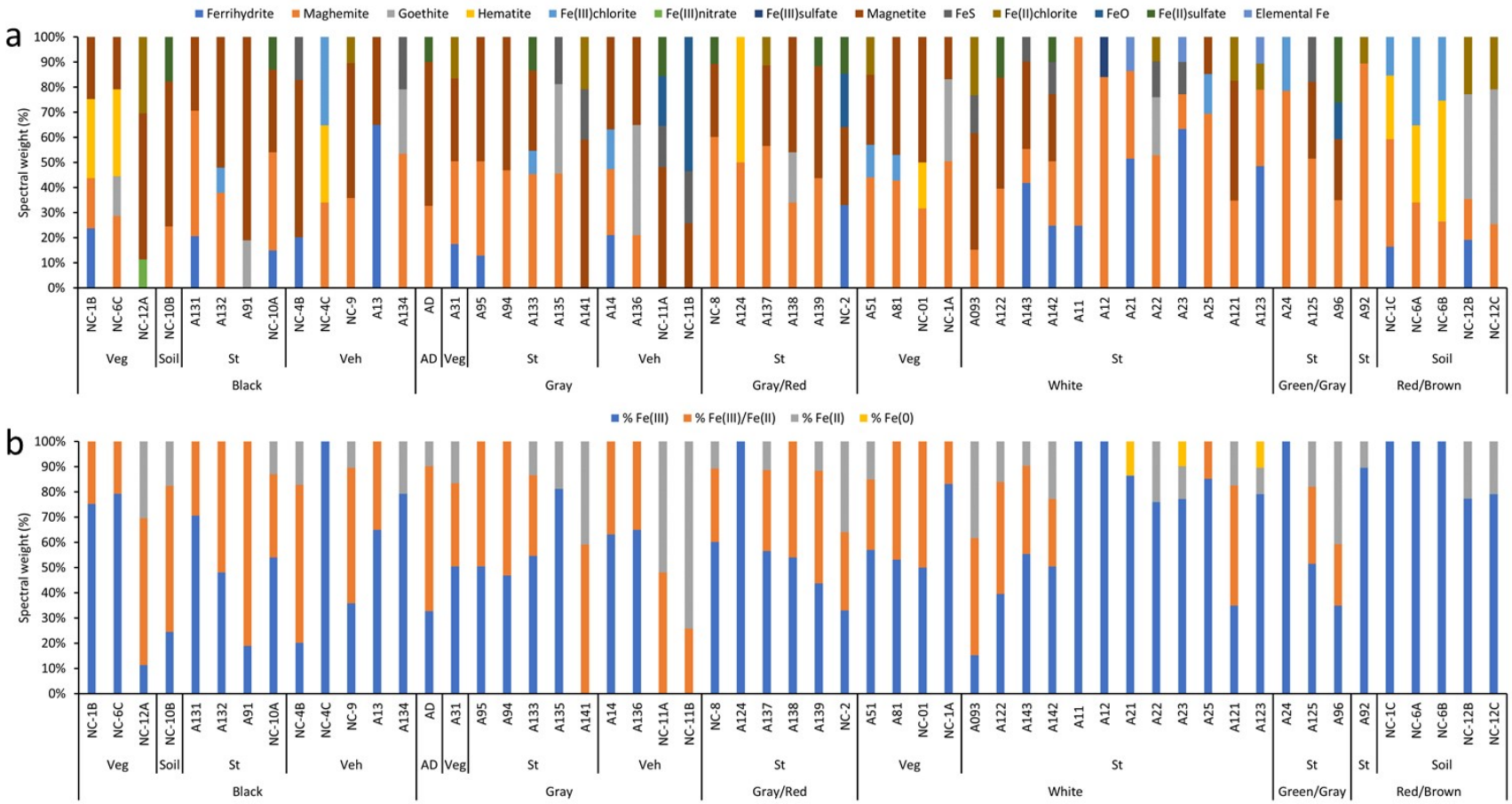

Figure S6. Percentage distribution of Fe species in ash samples determined by linear combination fitting analysis of Fe K-edge XANES (a). Estimated relative percentage of Fe oxidation states based on individual components determined from linear combination of XANES (b). Veg: vegetation, St: structure, Veh: vehicle, and AD: atmospheric deposition.

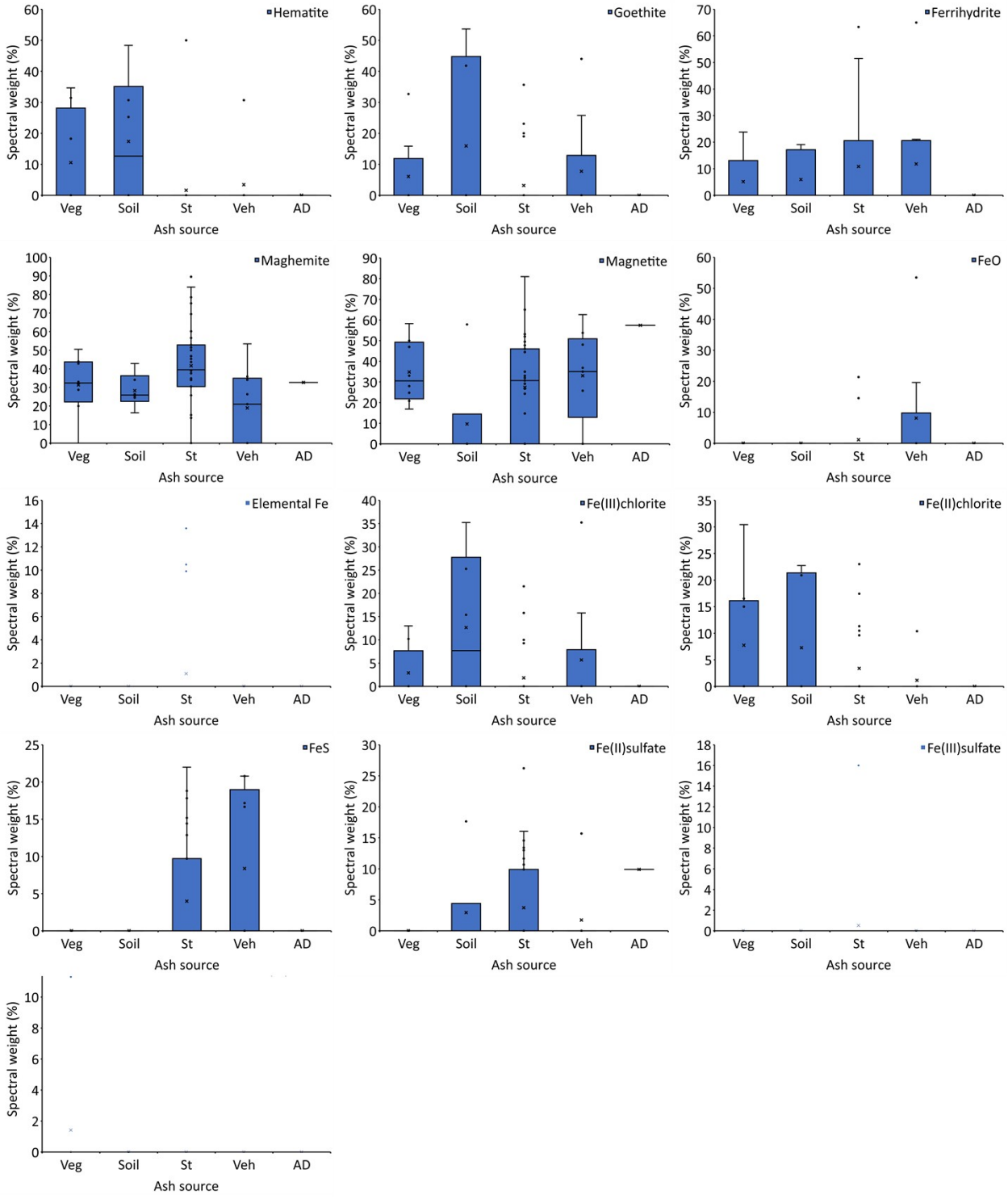

Figure S7. Iron phases as a function of ash source

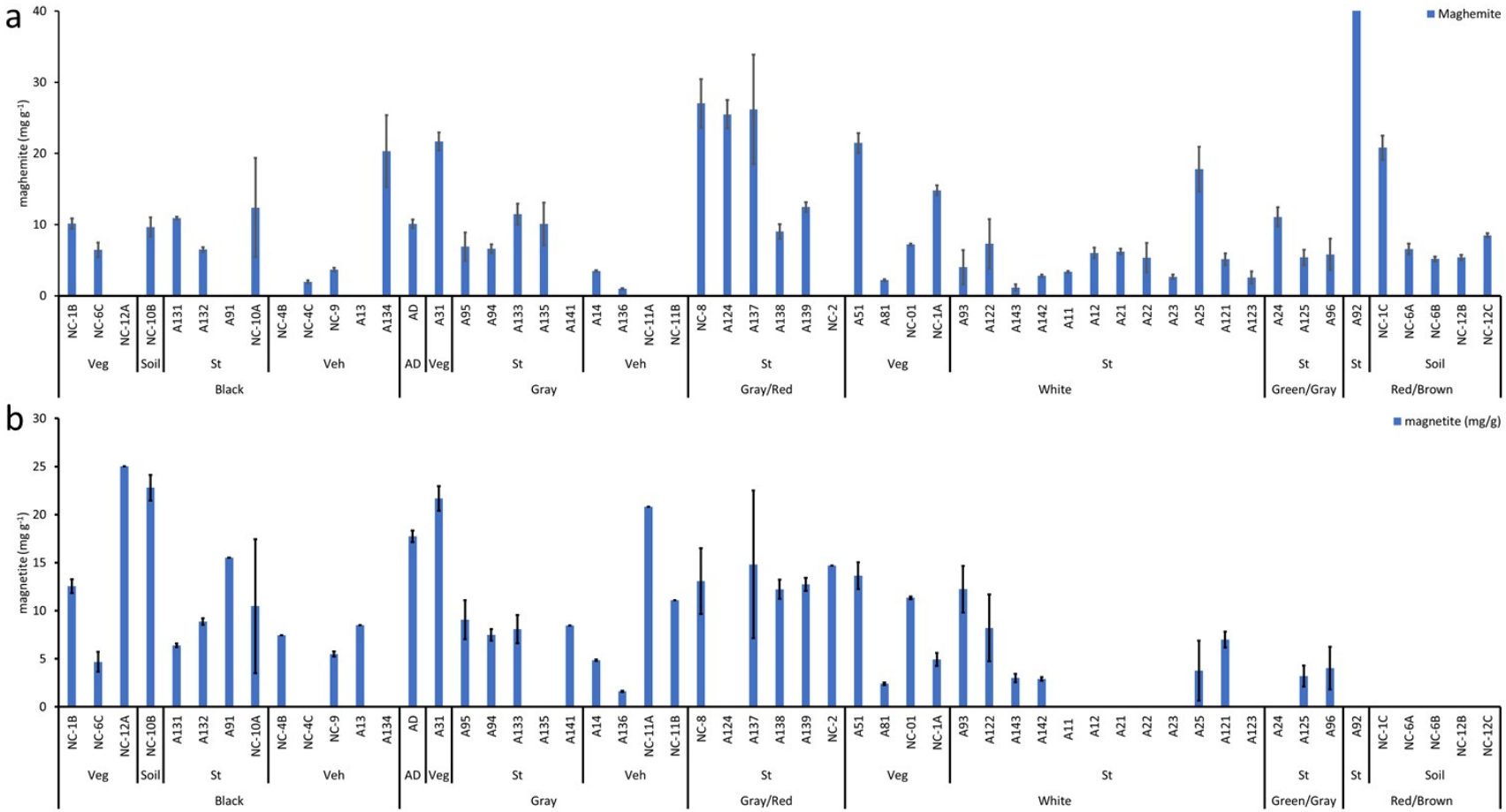
a
Maghemite
maghemite (mg g-1)
0
10
20
30
40
NC-1B NC-6C NC-12A NC-10B A131 A132 A91 NC-10A NC-4B NC-4C NC-9 A13 A134 AD A31 A95 A94 A133 A135 A141 A14 A136 NC-11A NC-11B NC-8 A124 A137 A138 A139 NC-2 A51 A81 NC-01 NC-1A A93 A122 A143 A142 A11 A12 A21 A22 A23 A25 A121 A123 A24 A125 A96 A92 NC-1C NC-6A NC-6B NC-12B NC-12C
Veg Soil St Veh AD Veg St Veh St Veg St St St Soil
Black Gray Gray/Red White Green/Gray Red/Brown
b
magnetite (mg/g)
magnetite (mg g-1)
0
5
10
15
20
25
30
NC-1B NC-6C NC-12A NC-10B A131 A132 A91 NC-10A NC-4B NC-4C NC-9 A13 A134 AD A31 A95 A94 A133 A135 A141 A14 A136 NC-11A NC-11B NC-8 A124 A137 A138 A139 NC-2 A51 A81 NC-01 NC-1A A93 A122 A143 A142 A11 A12 A21 A22 A23 A25 A121 A123 A24 A125 A96 A92 NC-1C NC-6A NC-6B NC-12B NC-12C
Veg Soil St Veh AD Veg St Veh St Veg St St St Soil
Black Gray Gray/Red White Green/Gray Red/Brown

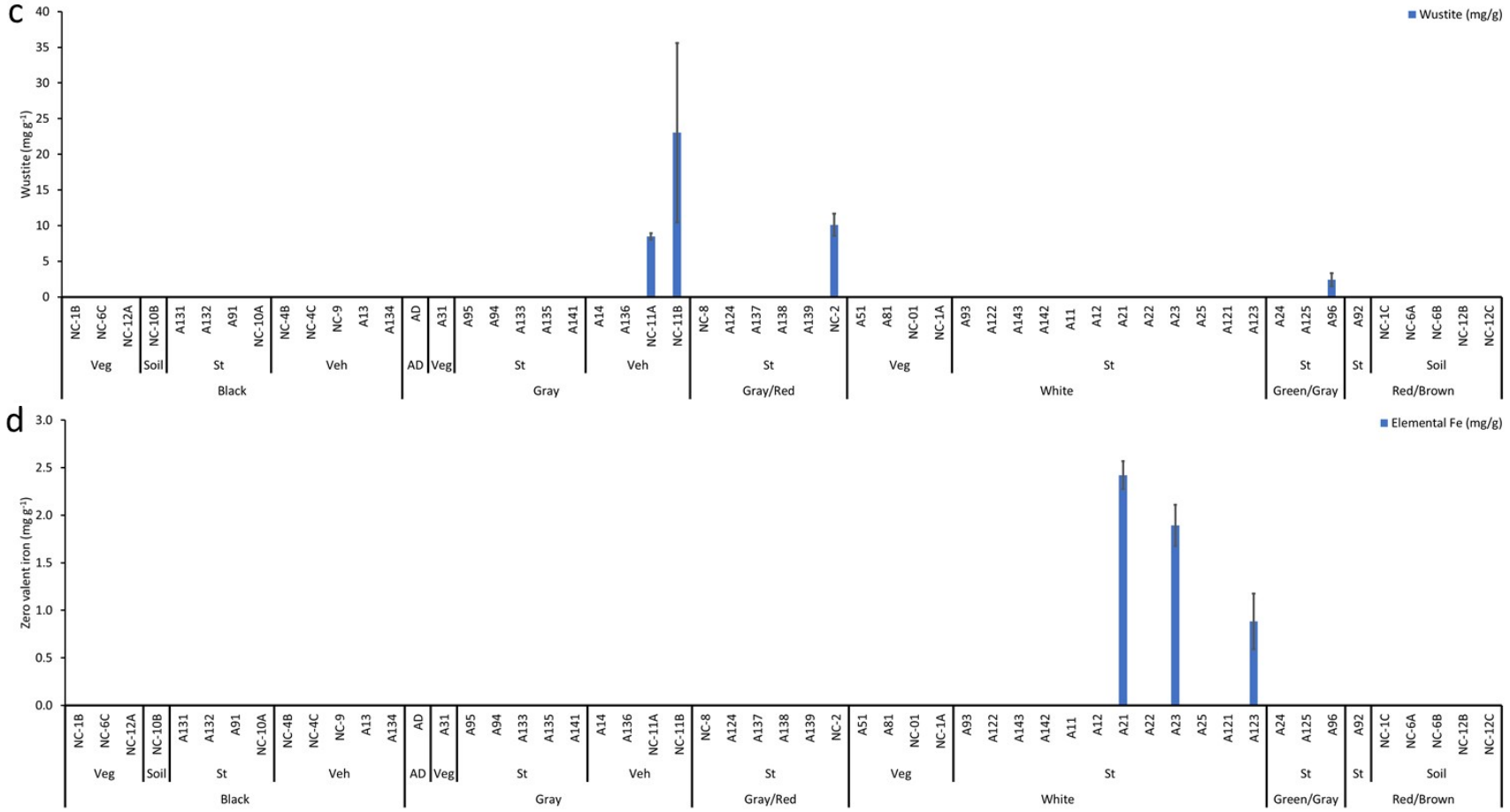

Figure S8. Iron speciation in ashes generated as a result of fire at the wildland-urban interface (a) maghemite, (b) magnetite, (c) wüstite, and (d) zero valent iron. Veg: vegetation, St: structure, Veh: vehicle, and AD: atmospheric deposition.

1. M. B. Bodí, D. A. Martin, V. N. Balfour, C. Santín, S. H. Doerr, P. Pereira, A. Cerdà and J. Mataix-Solera, Wildland fire ash: production, composition and eco-hydro-geomorphic effects, *Earth-Science Reviews*, 2014, **130**, 103-127.
2. Y. Wu, M. Fang, L. Lan, P. Zhang, K. V. Rao and Z. Bao, Rapid and direct magnetization of goethite ore roasted by biomass fuel, *Separation and Purification Technology*, 2012, **94**, 34-38.
3. R. Z. Abd Rashid, H. Mohd. Salleh, M. H. Ani, N. A. Yunus, T. Akiyama and H. Purwanto, Reduction of low grade iron ore pellet using palm kernel shell, *Renewable Energy*, 2014, **63**, 617-623.
4. Y. Yang, B. Chen, J. Hower, M. Schindler, C. Winkler, J. Brandt, R. Di Giulio, J. Ge, M. Liu, Y. Fu, L. Zhang, Y. Chen, S. Priya and M. F. Hochella, Discovery and ramifications of incidental Magnéli phase generation and release from industrial coal-burning, *Nature Communications*, 2017, **8**, 194.
5. D. K. McDaniel, V. M. Ringel-Scaia, H. A. Morrison, S. Coutermarsh-Ott, M. Council-Troche, J. W. Angle, J. B. Perry, G. Davis, W. Leng and V. Minarchick, Pulmonary exposure to Magnéli phase titanium suboxides results in significant macrophage abnormalities and decreased lung function, *Frontiers in immunology*, 2019, **10**, 2714.
6. M. F. Hochella, D. W. Mogk, J. Ranville, I. C. Allen, G. W. Luther, L. C. Marr, B. P. McGrail, M. Murayama, N. P. Qafoku and K. M. Rosso, Natural, incidental, and engineered nanomaterials and their impacts on the Earth system, *Science*, 2019, **363**.
7. R. J. Bixby, S. D. Cooper, R. E. Gresswell, L. E. Brown, C. N. Dahm and K. A. Dwire, Fire effects on aquatic ecosystems: an assessment of the current state of the science, *Freshwater Science*, 2015, **34**, 1340-1350.
8. J. D. Miller, H. Safford, M. Crimmins and A. E. Thode, Quantitative evidence for increasing forest fire severity in the Sierra Nevada and southern Cascade Mountains, California and Nevada, USA, *Ecosystems*, 2009, **12**, 16-32.
9. H. Chen, A. T. Chow, X.-W. Li, H.-G. Ni, R. A. Dahlgren, H. Zeng and J.-J. Wang, Wildfire burn intensity affects the quantity and speciation of polycyclic aromatic hydrocarbons in soils, *ACS Earth and Space Chemistry*, 2018, **2**, 1262-1270.
10. M. Scholze, W. Knorr, N. W. Arnell and I. C. Prentice, A climate-change risk analysis for world ecosystems, *Proceedings of the National Academy of Sciences*, 2006, **103**, 13116-13120.
11. K. D. Bladon, M. B. Emelko, U. Silins and M. Stone, Wildfire and the future of water supply.*Journal*, 2014.
12. D. Q. Brito, C. J. S. Passos, D. H. Muniz and E. C. Oliveira-Filho, Aquatic ecotoxicity of ashes from Brazilian savanna wildfires, *Environmental Science and Pollution Research*, 2017, **24**, 19671-19682.
13. T. C. Wegesser, K. E. Pinkerton and J. A. Last, California wildfires of 2008: coarse and fine particulate matter toxicity, *Environmental health perspectives*, 2009, **117**, 893-897.
14. Y. H. Kim, S. H. Warren, Q. T. Krantz, C. King, R. Jaskot, W. T. Preston, B. J. George, M. D. Hays, M. S. Landis and M. Higuchi, Mutagenicity and lung toxicity of smoldering vs. flaming emissions from various biomass fuels: implications for health effects from wildland fires, *Environmental health perspectives*, 2018, **126**, 017011.
15. R. Aguilera, T. Corringham, A. Gershunov and T. Benmarhnia, Wildfire smoke impacts respiratory health more than fine particles from other sources: observational evidence from Southern California, *Nature Communications*, 2021, **12**, 1493.
16. J. C. Liu, A. Wilson, L. J. Mickley, F. Dominici, K. Ebisu, Y. Wang, M. P. Sulprizio, R. D. Peng, X. Yue and J.-Y. Son, Wildfire-specific fine particulate matter and risk of hospital admissions in urban and rural counties, *Epidemiology (Cambridge, Mass.)*, 2017, **28**, 77.
17. A. Schuller and L. Montrose, Influence of Woodsmoke Exposure on Molecular Mechanisms Underlying Alzheimer's Disease: Existing Literature and Gaps in Our Understanding, *Epigenetics Insights*, 2020, **13**, 2516865720954873.

18. A. Oudin, D. Segersson, R. Adolfsson and B. Forsberg, Association between air pollution from residential wood burning and dementia incidence in a longitudinal study in Northern Sweden, *PLoS One*, 2018, **13**, e0198283.
19. E. Ormeno, B. Cespedes, I. A. Sanchez, A. Velasco-García, J. M. Moreno, C. Fernandez and V. Baldy, The relationship between terpenes and flammability of leaf litter, *Forest Ecology and Management*, 2009, **257**, 471-482.
20. S. Saura-Mas, S. Paula, J. Pausas and F. Lloret, Fuel loading and flammability in the Mediterranean Basin woody species with different post-fire regenerative strategies, *International Journal of Wildland Fire*, 2010, **19**, 783-794.
21. L. F. DeBano, D. G. Neary and P. F. Ffolliott, *Fire effects on ecosystems*, John Wiley & Sons, 1998.
22. T. Horie, F. Hauser and J. I. Schroeder, HKT transporter-mediated salinity resistance mechanisms in Arabidopsis and monocot crop plants, *Trends in Plant Science*, 2009, **14**, 660-668.
23. J. L. Jambor and J. E. Dutrizac, Occurrence and constitution of natural and synthetic ferrihydrite, a widespread iron oxyhydroxide, *Chemical Reviews*, 1998, **98**, 2549-2586.
24. M. Gajdardziska-Josifovska, R. G. McCLEAN, M. A. Schofield, C. V. Sommer and W. F. Kean, Discovery of nanocrystalline botanical magnetite, *European Journal of Mineralogy*, 2001, **13**, 863-870.
25. R. G. McClean and W. F. Kean, Contributions of wood ash magnetism to archaeomagnetic properties of fire pits and hearths, *Earth and Planetary Science Letters*, 1993, **119**, 387-394.
26. J. A. Ober, Mineral resource of the month: Iron oxide pigments, *Earth Magazine*, 2008.
27. United States Geological Survey, *Mineral commodity summaries 2021, 200 p., https://doi.org/10.3133/mcs2021.*, 2021.
28. G. P. Mastrotheodoros and K. G. Beltsios, Pigments—Iron-based red, yellow, and brown ochres, *Archaeological and Anthropological Sciences*, 2022, **14**, 35.
29. J. L. Till, B. Moskowitz and S. W. Poulton, Magnetic properties of plant ashes and their influence on magnetic signatures of fire in soils, *Frontiers in Earth Science*, 2021, **8**.
30. N. Jordanova, D. Jordanova and V. Barrón, Wildfire severity: Environmental effects revealed by soil magnetic properties, *Land Degradation & Development*, 2019, **30**, 2226-2242.
31. B. A. Maher, I. A. M. Ahmed, V. Karloukovski, D. A. MacLaren, P. G. Foulds, D. Allsop, D. M. A. Mann, R. Torres-Jardón and L. Calderon-Garciduenas, Magnetite pollution nanoparticles in the human brain, *Proceedings of the National Academy of Sciences*, 2016, **113**, 10797-10801.
32. D. Lu, Q. Luo, R. Chen, Y. Zhuansun, J. Jiang, W. Wang, X. Yang, L. Zhang, X. Liu, F. Li, Q. Liu and G. Jiang, Chemical multi-fingerprinting of exogenous ultrafine particles in human serum and pleural effusion, *Nature Communications*, 2020, **11**, 2567.
33. L. Calderón-Garcidueñas, A. González-Maciel, P. S. Mukherjee, R. Reynoso-Robles, B. Pérez-Guillé, C. Gayosso-Chávez, R. Torres-Jardón, J. V. Cross, I. A. M. Ahmed, V. V. Karloukovski and B. A. Maher, Combustion- and friction-derived magnetic air pollution nanoparticles in human hearts, *Environmental Research*, 2019, **176**, 108567.
34. M. Könczöl, S. Ebeling, E. Goldenberg, F. Treude, R. Gminski, R. Gieré, B. Grobéty, B. Rothen-Rutishauser, I. Merfort and V. Mersch-Sundermann, Cytotoxicity and Genotoxicity of Size-Fractionated Iron Oxide (Magnetite) in A549 Human Lung Epithelial Cells: Role of ROS, JNK, and NF-κB, *Chemical Research in Toxicology*, 2011, **24**, 1460-1475.
35. Q. Pankhurst, D. Hautot, N. Khan and J. Dobson, Increased Levels of Magnetic Iron Compounds in Alzheimer's Disease, *Journal of Alzheimer's Disease*, 2008, **13**, 49-52.
36. D. Hautot, Q. A. Pankhurst, N. Khan and J. Dobson, Preliminary evaluation of nanoscale biogenic magnetite in Alzheimer's disease brain tissue, *Proceedings of the Royal Society of London. Series B: Biological Sciences*, 2003, **270**, S62-S64.

37. W. Tang, J. Llort, J. Weis, M. M. G. Perron, S. Basart, Z. Li, S. Sathyendranath, T. Jackson, E. Sanz Rodriguez, B. C. Proemse, A. R. Bowie, C. Schallenberg, P. G. Strutton, R. Matear and N. Cassar, Widespread phytoplankton blooms triggered by 2019–2020 Australian wildfires, *Nature*, 2021, **597**, 370-375.
38. A. Ito, Y. Ye, C. Baldo and Z. Shi, Ocean fertilization by pyrogenic aerosol iron, *npj Climate and Atmospheric Science*, 2021, **4**, 30.
39. N. Moteki, K. Adachi, S. Ohata, A. Yoshida, T. Harigaya, M. Koike and Y. Kondo, Anthropogenic iron oxide aerosols enhance atmospheric heating, *Nature Communications*, 2017, **8**, 1-11.
40. H. Matsui, N. M. Mahowald, N. Moteki, D. S. Hamilton, S. Ohata, A. Yoshida, M. Koike, R. A. Scanza and M. G. Flanner, Anthropogenic combustion iron as a complex climate forcer, *Nature Communications*, 2018, **9**, 1593-1593.
41. inciweb, *Incident information system. North Complex.* https://inciweb.nwcg.gov/incident/6997/ 2022.
42. United States Department of Agriculture, *Burned-area report: North complex.*, Report FS-2500-8 (2/20), United States Department of Agriculture FOREST SERVICE, 2020.
43. CALFire, *LNU Lightning Complex (includes Hennessey, Gamble, 15-10, Spanish, Markley, 13-4, 11-16, Walbridge) Incident.* https://www.fire.ca.gov/incidents/2020/8/17/lnu-lightning-complex-includes-hennessey-gamble-15-10-spanish-markley-13-4-11-16-walbridge/, 2022.
44. E. Welter, R. Chernikov, M. Herrmann and R. Nemausat, A beamline for bulk sample x-ray absorption spectroscopy at the high brilliance storage ring PETRA III, *AIP Conference Proceedings*, 2019, **2054**, 040002.
45. M. Newville, Larch: an analysis package for XAFS and related spectroscopies, *Journal of Physics: Conference Series*, 2013, **430**, 012007.
46. M. Desmau, A python library to read, process and analyze X-ray absorption spectra. https://github.com/marcoalsina/araucaria.).
47. S. Van Der Walt, S. C. Colbert and G. Varoquaux, The NumPy array: a structure for efficient numerical computation, *Computing in Science & Engineering*, 2011, **13**, 22-30.
48. P. Virtanen, R. Gommers, T. E. Oliphant, M. Haberland, T. Reddy, D. Cournapeau, E. Burovski, P. Peterson, W. Weckesser and J. Bright, SciPy 1.0: fundamental algorithms for scientific computing in Python, *Nature Methods*, 2020, **17**, 261-272.
49. J. D. Hunter, Matplotlib: A 2D graphics environment, *Computing in Science & Engineering*, 2007, **9**, 90-95.
50. U. Schwertmann and R. M. Cornell, *Iron oxides in the laboratory: preparation and characterization*, John Wiley & Sons, 2008.
51. U. Schwertmann, P. Cambier and E. Murad, Properties of goethites of varying crystallinity, *Clays and Clay Minerals*, 1985, **33**, 369-378.
52. M. Desmau, M. A. Alsina and J.-F. Gaillard, XAS study of Sn speciation in toothpaste, *Journal of Analytical Atomic Spectrometry*, 2021, **36**, 407-415.
53. C. Da Silva-Cadoux, L. Zanella and J.-F. Gaillard, Selecting reference compounds for determining chemical speciation by X-ray absorption spectroscopy, *Journal of Analytical Atomic Spectrometry*, 2012, **27**, 957-965.
54. M. Newville, T. Stensitzki, D. B. Allen, M. Rawlik, A. Ingargiola and A. Nelson, LMFIT: Non-linear least-square minimization and curve-fitting for Python, *Astrophysics Source Code Library*, 2016, ascl: 1606.1014.
55. J. G. Chen, NEXAFS investigations of transition metal oxides, nitrides, carbides, sulfides and other interstitial compounds, *Surface Science Reports*, 1997, **30**, 1-152.
56. E. Doelsch, I. Basile-Doelsch, J. Rose, A. Masion, D. Borschneck, J.-L. Hazemann, H. Saint Macary and J.-Y. Bottero, New combination of EXAFS spectroscopy and density fractionation for the

speciation of chromium within an andosol, *Environmental Science & Technology*, 2006, **40**, 7602-7608.
57. M. Munoz, V. De Andrade, O. Vidal, E. Lewin, S. Pascarelli and J. Susini, Redox and speciation micromapping using dispersive X-ray absorption spectroscopy: Application to iron in chlorite mineral of a metamorphic rock thin section, *Geochemistry, Geophysics, Geosystems*, 2006, **7**.
58. T. Gonet, B. A. Maher and J. Kukutschová, Source apportionment of magnetite particles in roadside airborne particulate matter, *Science of The Total Environment*, 2021, **752**, 141828.
59. A. R. Muxworthy, J. Matzka, A. F. Davila and N. Petersen, Magnetic signature of daily sampled urban atmospheric particles, *Atmospheric Environment*, 2003, **37**, 4163-4169.
60. A. R. Muxworthy, J. Matzka and N. Petersen, Comparison of magnetic parameters of urban atmospheric particulate matter with pollution and meteorological data, *Atmospheric Environment*, 2001, **35**, 4379-4386.
61. Q. Zhang, D. Lu, D. Wang, X. Yang, P. Zuo, H. Yang, Q. Fu, Q. Liu and G. Jiang, Separation and Tracing of Anthropogenic Magnetite Nanoparticles in the Urban Atmosphere, *Environmental Science & Technology*, 2020, **54**, 9274-9284.
62. U. Schwertmann, *Occurrence and formation of iron oxides in various pedoenvironments. In Iron in soils and clay minerals. 11. 267-308.*, D. Reidek Publishing Company, Boston, 1988.
63. V. P. Ponomar, T. S. Antonenko, O. A. Vyshnevskyi and A. B. Brik, Thermally induced changes in the magnetic properties of iron oxide nanoparticles under reducing and oxidizing conditions, *Advanced Powder Technology*, 2020, **31**, 2587-2596.
64. M. S. Ellid, Y. S. Murayed, M. S. Zoto, S. Musić and S. Popović, Chemical reduction of hematite with starch, *Journal of Radioanalytical and Nuclear Chemistry*, 2003, **258**, 299-305.
65. V. P. Ponomar, N. O. Dudchenko and A. B. Brik, Reduction roasting of hematite to magnetite using carbohydrates, *International Journal of Mineral Processing*, 2017, **164**, 21-25.
66. M. Hanesch, H. Stanjek and N. Petersen, Thermomagnetic measurements of soil iron minerals: the role of organic carbon, *Geophysical Journal International*, 2006, **165**, 53-61.
67. A. Gehring and A. Hofmeister, The transformation of lepidocrocite during heating: a magnetic and spectroscopic study, *Clays and Clay Minerals*, 1994, **42**, 409-415.
68. T. S. Gendler, V. P. Shcherbakov, M. J. Dekkers, A. K. Gapeev, S. K. Gribov and E. McClelland, The lepidocrocite–maghemite–haematite reaction chain—I. Acquisition of chemical remanent magnetization by maghemite, its magnetic properties and thermal stability, *Geophysical Journal International*, 2005, **160**, 815-832.
69. M. Valix and W. Cheung, Study of phase transformation of laterite ores at high temperature, *Minerals Engineering*, 2002, **15**, 607-612.
70. Q. Y. Wang, Y. Wu, Y. H. Li and X. Yang, Biomass reduction roasting-magnetic separation of low grade goethite, *Materials Science Forum*, 2015, **814**, 235-240.
71. W. Cheung and M. Valix, Selective Reduction Roasting of Limonite Ores: Effect of Over-reduction, *Proceedings of XXIV International Mineral Processing Congress*, 2008, 2951-2957.
72. V. P. Ponomar, Thermomagnetic properties of the goethite transformation during high-temperature treatment, *Minerals Engineering*, 2018, **127**, 143-152.
73. S. Luo, C. Yi and Y. Zhou, Direct reduction of mixed biomass-Fe2O3 briquettes using biomass-generated syngas, *Renewable Energy*, 2011, **36**, 3332-3336.
74. M. Kumar, S. Nath and S. K. Patel, Studies on the reduction–swelling behaviors of hematite iron ore pellets with noncoking coal, *Mineral Processing & Extractive Metallurgy Review*, 2010, **31**, 256-268.
75. D. T. Gottuk, R. J. Roby and C. L. Beyler, The role of temperature on carbon monoxide production in compartment fires, *Fire Safety Journal*, 1995, **24**, 315-331.

76. Q. Xu, W. Peng and C. Ling, An experimental analysis of soybean straw combustion on both CO and NOx emission characteristics in a tubular furnace, *Energies*, 2020, **13**, 1587.
77. K. Przepiera and A. Przepiera, Kinetics of thermal transformations of precipitated magnetite and goethite, *Journal of Thermal Analysis and Calorimetry*, 2001, **65**, 497-503.
78. M. J. Molaei, A. Ataie, S. Raygan and S. J. Picken, The effect of different carbon reducing agents in synthesizing barium ferrite/magnetite nanocomposites, *Materials Chemistry and Physics*, 2018, **219**, 155-161.
79. B. A. Maher, Airborne magnetite-and iron-rich pollution nanoparticles: potential neurotoxicants and environmental risk factors for neurodegenerative disease, including Alzheimer's disease, *Journal of Alzheimer's Disease*, 2019, **71**, 361-375.
80. J. C. Liu, L. J. Mickley, M. P. Sulprizio, F. Dominici, X. Yue, K. Ebisu, G. B. Anderson, R. F. A. Khan, M. A. Bravo and M. L. Bell, Particulate air pollution from wildfires in the Western US under climate change, *Climatic Change*, 2016, **138**, 655-666.
81. S. Sharma, M. Chandra and S. H. Kota, Health Effects Associated with PM2.5: a Systematic Review, *Current Pollution Reports*, 2020, **6**, 345-367.
82. J. Kaiser, A. Heil, M. Andreae, A. Benedetti, N. Chubarova, L. Jones, J.-J. Morcrette, M. Razinger, M. Schultz and M. Suttie, Biomass burning emissions estimated with a global fire assimilation system based on observed fire radiative power, *Biogeosciences*, 2012, **9**, 527-554.
83. J. Xing, J. Pleim, R. Mathur, G. Pouliot, C. Hogrefe, C.-M. Gan and C. Wei, Historical gaseous and primary aerosol emissions in the United States from 1990 to 2010, *Atmospheric Chemistry and Physics*, 2013, **13**, 7531-7549.
84. R. Munoz-Alpizar, R. Pavlovic, M. D. Moran, J. Chen, S. Gravel, S. B. Henderson, S. Ménard, J. Racine, A. Duhamel and S. Gilbert, Multi-year (2013–2016) PM2. 5 wildfire pollution exposure over North America as determined from operational air quality forecasts, *Atmosphere*, 2017, **8**, 179.
85. United States Environmental Protection Agency, *Draft Guidance for Comment: Significant Impact Levels for Ozone and Fine Particle in the Prevention of Significant Deterioration Permitting Program. 2016; p. 13. Available online: https://www.epa.gov/sites/production/files/2016-08/documents/pm2_5_sils_and_ozone_draft_guidance.pdf (accessed on 18 February 2022).* 2016.
86. B. Ford, M. Val Martin, S. Zelasky, E. Fischer, S. Anenberg, C. L. Heald and J. Pierce, Future fire impacts on smoke concentrations, visibility, and health in the contiguous United States, *GeoHealth*, 2018, **2**, 229-247.
87. P. N. Sedwick, E. R. Sholkovitz and T. M. Church, Impact of anthropogenic combustion emissions on the fractional solubility of aerosol iron: Evidence from the Sargasso Sea, *Geochemistry, Geophysics, Geosystems*, 2007, **8**.
88. B. H. Samset, C. W. Stjern, E. Andrews, R. A. Kahn, G. Myhre, M. Schulz and G. L. Schuster, Aerosol Absorption: Progress Towards Global and Regional Constraints, *Current Climate Change Reports*, 2018, **4**, 65-83.
89. C. Baldo, P. Formenti, S. Nowak, S. Chevaillier, M. Cazaunau, E. Pangui, C. Di Biagio, J. F. Doussin, K. Ignatyev, P. Dagsson-Waldhauserova, O. Arnalds, A. R. MacKenzie and Z. Shi, Distinct chemical and mineralogical composition of Icelandic dust compared to northern African and Asian dust, *Atmos. Chem. Phys.*, 2020, **20**, 13521-13539.
90. R. W. Bergstrom Jr, Predictions of the spectral absorption and extinction coefficients of an urban air pollution aerosol model, *Atmospheric Environment (1967)*, 1972, **6**, 247-258.
91. J. M. Greenberg and H. C. van de Hulst, *Interstellar dust and related topics*, Springer Science & Business Media, 2012.

92. K. D. Lamb, H. Matsui, J. M. Katich, A. E. Perring, J. R. Spackman, B. Weinzierl, M. Dollner and J. P. Schwarz, Global-scale constraints on light-absorbing anthropogenic iron oxide aerosols, *npj Climate and Atmospheric Science*, 2021, **4**, 15.
93. G. Kletetschka and S. K. Banerjee, Magnetic stratigraphy of Chinese loess as a record of natural fires, *Geophysical Research Letters*, 1995, **22**, 1341-1343.
94. Natural Resources Conservation Service, *Soil Series Classification Database. U.S. Department of Agriculture (accessed April 6, 2022).* *https://www.nrcs.usda.gov/wps/portal/nrcs/detail/soils/survey/class/data/?cid=nrcs142p2_053583*.